HHS Public Access

Author manuscript

*Acta Biomater*. Author manuscript; available in PMC 2019 September 15.

Published in final edited form as:

*Acta Biomater*. 2018 September 15; 78: 308–319. doi:10.1016/j.actbio.2018.07.017.

# The mechanical response of the mouse cervix to tensile cyclic loading in term and preterm pregnancy

**C. Jayyosi**[a], **N. Lee**[a], **A. Willcockson**[b], **S. Nallasamy**[b], **M. Mahendroo**[b], and **K. Myers**[a,*]

[a]Department of Mechanical Engineering, Columbia University, New York, NY, 10027, USA

[b]Department of Obstetrics and Gynecology and Green Center for Reproductive Biological Sciences, University of Texas Southwestern Medical Center, Dallas, TX, 75390, USA

## Abstract

A well-timed modification of both the collagen and elastic fiber network in the cervix during pregnancy accompanies the evolution of tissue mechanical parameters that are key to a successful pregnancy. Understanding of the cervical mechanical behaviour along normal and abnormal pregnancy is crucial to define the molecular events that regulate remodeling in term and preterm birth (PTB). In this study, we measured the mechanical response of mouse cervical tissue to a history of cyclic loading and quantified the tissues ability to recover from small and large deformations. Assessments were made in nonpregnant, pregnant (gestation days 6, 12, 15 and 18) and mouse models of infection mediated PTB treated with lipopolysaccharide on gestation d15 (LPS treated) and hormone withdrawal mediated PTB on gestation d15 (RU486 treated). The current study uncovers the contributions of collagen and elastic fiber networks to the progressive change in mechanical function of the cervix through pregnancy. Premature cervical remodeling induced on gestation day 15 in the LPS infection model is characterized by distinct mechanical properties that are similar but not identical to mechanical properties at term ripening on day 18. Remodeling in the LPS infection model results in a weaker cervix, unable to withstand high loads. In contrast, the RU486 preterm model resembles the cyclic mechanical behaviour seen for term d18 cervix, where the extremely compliant tissue is able to withstand multiple cycles under large deformations without breaking. The distinct material responses to load-unload cycles in the two PTB models matches the differing microstructural changes in collagen and elastic fibers in these two models of preterm birth. Improved understanding of the impact of microstructural changes to mechanical performance of the cervix will provide insights to aid in the development of therapies for prevention of preterm birth.

### Keywords

preterm birth; cervical remodeling; cyclic tensile test; LPS; RU486

*Corresponding author, 500 W 120th street, Mudd 220, New York, NY, 10027, kmm2233@columbia.edu (K. Myers).

7.·Conflict of interest

None of the authors have any professional or financial conflict of interest.

## 1. Introduction

Preterm Birth (PTB), defined as a delivery before 37 weeks of gestation, remains an important clinical challenge. It impacts approximately 12% of all births [1] (9.6% in the US in 2015 [2]), with over 15 million babies affected every year worldwide[3]. The PTB rate significantly contributes to infant mortality and lifelong health consequences in some survivors [4]. An understanding of causes and etiologies remains incomplete and few studies link biologic, chemical, and mechanical factors to overall tissue function. Thus, there is still much to be learned in order to implement successful therapies or improve the ones currently used [5].

Over the course of pregnancy, the uterine cervix undergoes important structural and mechanical changes [6]. This process, known as cervical remodeling, ensures the transformation of the cervix from a strong barrier, which protects and prevents the fetus from passing into the birth canal, to a compliant structure that can significantly dilate to allow for a successful delivery [7]. Understanding the functional mechanisms of cervical remodeling is then required for the development of early, accurate diagnostic methods for PTB and improved targeted therapies addressing patient-specific etiologies.

Taking advantage of the similarities between the human and rodent cervix [8, 7, 9], the ability to obtain cervical samples at all time points in pregnancy, and the relatively short gestational period in rodents (19–21 days), numerous mechanical testing methodologies have been implemented in mice and rats to characterize the highly hyperviscoelastic mechanical behavior of the cervix through pregnancy [10, 11, 12, 13]. In mice, cervical softening, defined by a drop in tissue stiffness relative to non-pregnant (NP), is detectable by gestation day 12 and thereafter declines such that cervical stiffness is 20 times reduced at term before labor on gestation day 18 as compared to the NP cervix [14, 12, 15]. This softening is not homogeneous during pregnancy, since the rate of stiffness decline is most pronounced between day 6 and day 12, followed by a less drastic continuous softening until day 15, while a minor stiffness drop is observed in late pregnancy between day 15 and day 18 [16, 17, 12]. While the tangent stiffness of the mechanical response between day 15 and day 18 is not altered much, the swelling behavior of the tissue is postulated to change significantly given the important increase in hyaluronan (HA a non-sulfated glycosaminoglycan of the extracellular matrix) during this time [18]. Hence, the material property changes between day 15 and day 18 remain to be determined. Similar to cervical stiffness, the mechanical strength of pregnant mouse cervix undergoes a dramatic decrease by day 12 with a less pronounced decrease in late gestation [12, 15].

As a load-bearing soft tissue, the mechanical properties of the cervix are linked to the composition and organization of its extracellular matrix (ECM) [19, 17]. Significant remodeling of the cervical ECM over the course of pregnancy is achieved, in part by modification of the collagen fiber network [20]. Microscopic imaging of the collagen network during pregnancy reveal a dynamic remodeling from straight fibers for non-pregnant tissue to thicker, crimped fibers for pregnant tissues [21, 22], in both human and mouse cervices. Cervical collagen also undergoes a turnover during pregnancy where mature

cross-linked collagen is progressively replaced by immature less cross-linked collagen [17] while total collagen content remains the same [23, 14].

While the evolution of cervical mechanical parameters through pregnancy is primarily equated with the progressive change in processing, assembly and turnover of collagen fibers [8], recent studies from our group suggest that elastic fiber remodeling may also contribute to mechanical behavior in cervical remodeling [15]. Elastic fiber ultrastructure is observed to change from long and straight fibers in the NP to progressively shorter and randomly oriented fibers on gestation day 18. Uni-axial tensile tests on cervices of mice with structural defects in elastic fibers exhibit overall degraded mechanical properties [15]. The importance of understanding the collective contributions of both collagen and elastic fibers to the mechanical behavior of the cervix is also supported by our recent studies demonstrating a change in collagen fiber morphology by second harmonic generation (SHG) and disruption of elastic fiber ultrastructure by transmission electron microscopy, in the subepithelial stroma of mice undergoing inflammation-induced premature cervical ripening [24, 25](see figure in discussion).

Two established mouse models of premature cervical remodeling and PTB are infection-mediated and progesterone withdrawal-mediated, achieved by the administration of lipopolysaccharide (LPS) or mifepristone (RU486), respectively. Cervical ripening induced by LPS treatment is achieved by a transcriptional pathway that is distinct from term ripening [26, 24], and noted structural changes in collagen and elastic fibers are hypothesized to result from the increased expression of ECM-degrading proteases and proinflammatory genes. In contrast, RU486-mediated ripening is most similar to term ripening [26]. Since mifepristone is a progesterone antagonist, mice treated with RU486 experience a withdrawal of progesterone similar to the pathway for term ripening on day 18.

Previously published uni-axial load-to-break mechanical tests suggest a decline in tissue stiffness in LPS and RU486-treated mice similar to term before labor [27]. Given the difficulty in conducting mechanical tests on such a small, curved tissue sample, these load-to-break tests provide the necessary starting point for mechanical characterization. However, these tests provide an incomplete picture of the individual contributions of collagen and elastic fiber remodeling to the hyperviscoelastic mechanical behavior of the non-pregnant and pregnant cervix. In addition, they do not accurately reflect the repetitive loadunload that the cervix experiences with acute loading from the fetus or with labor. Therefore, we developed a load-unload cyclic mechanical test for the mouse cervix to tease out specific contributions of the collagen or elastic fibers to the mechanical behavior [28]. Further, we investigate the evolving damage state of the ECM and its ability to recoil back to an undeformed state after loading [29, 30].

Therefore, the aims of this study are: 1) to provide a detailed characterization of cervical mechanical properties at different time points during a normal pregnancy with a focus on parameters that quantify the ability of the cervix to recover from loading; 2) to characterize the mechanical differences between normal day 15, day 18 tissues and premature remodeling induced on day 15 by LPS or RU486, and link those mechanical parameters to microstructural considerations to better identify key factors in the apparition of PTB

disorders. Here, we report the biomechanical load-unload signature of normal tissue remodeling in a murine pregnancy and show that infection-mediated premature cervical remodeling is functionally distinct from term and hormone withdrawal-mediated preterm remodeling.

## 2. Material and methods

### 2.1 Mouse cervix collection

All animal studies were approved by the University of Texas Southwestern Medical Center Institutional Animal Care and Research Advisory Committee. The breeding and tissue collection were performed at the University of Texas Southwestern Medical Center (Dallas, TX). C57B6/129sv wild-type (WT) mice were housed under a 12h light/12h dark cycle at 22°C. Pregnancy was detected with the presence of a vaginal plug (considered day 0), with birth usually occurring on early morning of day 19. Non-pregnant (NP), gestation day 6 (d6), day 12 (d12), day 15 (d15) and day 18 (d18) reproductive tracts were collected (n=5 per gestation group) and immediately frozen to be shipped overnight to Columbia University on dry ice. Tissues were then stored at −80°C until test day.

PTB models were generated following the procedure described in Holt *et al.* [26]. Briefly, for the infection mediated treatment, mice were anesthetized on early morning of gestation d15 and a small incision was made in the abdomen to access the uterus. An injection of 150$\mu$g of LPS (O55:B5, Sigma, St; Louis, MO) dissolved in 30$\mu$l of sterile water was administered into the uterus between two fetal sacs. The incision was then closed with wound clips and 0.1$\mu$g/kg buprenorphine (Hospira, Lake Forest, Illinois) was administered for pain relief. Since the intrauterine injection of LPS leads to preterm delivery approximately 7–8h post-surgery [26], mice were sacrificed 6h after the injection. An LPS sham group was also created through the same procedure with an injection of 30$\mu$l of sterile water.

For the progesterone withdrawal model, a subcutaneous injection of 0.5mg of RU486 (Sigma) in glyceryl trioleate (Sigma, St Louis) was administered on the evening of gestation day 14. Mice were sacrificed 12 hours post injection (hence on day 15), since RU486 causes premature cervical ripening and preterm birth 13–16 hours after injection [31]. The need for a RU486 sham group was ruled out in a previous study [26] showing that there was no trauma following the mifepristone injection contrary to the surgery required for the LPS treatment. The reproductive tracts of 5 animals per group were collected and shipped to Columbia University for mechanical testing as previously described.

### 2.2. Sample preparation

The sample preparation and mechanical set up have been previously described in Yoshida *et al.* [10]. Briefly, on test day, the sample was thawed in phosphate buffered saline (PBS) with 2mM ethylenediamineteraacetic acid (EDTA). The complete reproductive tract was dissected under an optical microscope to isolate the cervix and remove the attached vaginal wall. The cervix was then mounted on custom grips by passing two surgical sutures through the cervical canal (Fig. 1). The ensemble was placed in an hydration bath (PBS + 2mM

EDTA solution) on a universal testing machine (Model 5948 MicroTester Instron, 10N load cell, resolution 0.0025N) (Fig. 1) and allowed to swell to equilibrium at room temperature for 3h. This swelling to equilibrium step ensured that the geometry changes recorded during the mechanical test were not influenced by any changes in swelling dynamics [11].

### 2.3. Mechanical testing set up

Samples were subjected to a cyclic tensile test. The loading regimen (Fig. 2) consisted of five series, each at different load levels. Each series consisted of three load-unload cycles separated by pauses of 20min for recovery. To set up the test, after the 3h swelling period, a small pre-load of 0.001N was applied to make sure both sutures were in contact with the inner side of the cervical canal.A first image was taken at this point which defined our reference configuration for the test. Loading was then conducted at a grip-to-grip displacement rate of 0.1mm/s. Given the broad range in mechanical properties between the NP cervix, and early, mid or late pregnancy, the range of load levels used were scaled according to the overall estimated stiffness of defined groups. Based on preliminary tests, the specimens were split into three loading groups: the NP/early pregnancy group including the NP and d6 samples was loaded to 0.05N, 0.5N, 1N, 1.5N and 2N; the mid pregnancy group included the d12 samples and was loaded to 0.05N, 0.2N, 0.4N, 0.6N and 0.8N; the late pregnancy group included gestation day d15, d18, d15-LPS sham, d15-LPS and d15-RU486 samples and was loaded to 0.05N, 0.1N, 0.2N, 0.3N and 0.4N (Fig. 2). Finally, after the samples were subjected to the five series of increasing load levels, those that didn't break during cyclic loading were loaded to failure. Behavior comparisons were only made between specimens within the same loading group, or between parameters calculated on the very first load series since it is common for all loading groups.

During testing, the changes of sample geometry were recorded using two CCD camera (Point Grey Grasshopper, GRAS- 50S5M-C 75mm, f/4 lens) tracking the front and side view of the cervix (Fig. 1bc). The image acquisition rate was set to 1 image every 0.1mm of displacement during the cycles and 1 image/2min during the recovery periods. After the test was completed, the cameras were calibrated to get the pixel to mm ratio using a high resolution ruler (0.4 mm resolution).

### 2·4. Data processing

From the total set of acquired images, a subset of images per cycles were chosen for image analysis. Seven images on the first and third cycles of each series were analyzed (3 images during the load, 3 during unload and the one at the apex). The images were automatically segmented using a custom MATLAB script, to get the average length [$l$], height [$h$], width [$w$] and cervical opening [$co$] (Fig. 3). Cervical measurements were then linearly interpolated between the time points to match the Force [F] and Extension data acquisition rate. From there, the averaged Cauchy stress and stretch were computed in the traction direction $\vec{y}$ as:

$$\sigma_{yy} = \frac{F}{(l) \cdot (w)}$$

$$\lambda_y = \frac{co}{co_{init}}$$

To quantify the evolving damage mechanical state of the samples during testing, we measured several mechanical parameters for every series and cycles (Fig. 4b). The stretch shift $\Delta\lambda$ is defined as the difference between the peak stretches of cycle 3 and cycle 1 for each series. It is therefore an indication of the permanent deformation of the tissue after loading, and thus gives insight about the performance of the elastic part of the ECM, and the irreversible sliding of collagen fibers. It is noteworthy that this damage parameter includes a combination of various deformation mechanisms inducing permanent deformation of the tissue, such as irreversible sliding and/or uncrimping of collagen fibers through elongation/breakage of crosslinks, and possibly some fiber breakage at the higher load levels considered. The stretch shift may also include the contribution of preconditioning effects and the Mullins effect, usually observed in soft tissues.

We also computed the modulus at low stretch $E_0$ and the maximum modulus on the load curve $E_{max}$ to assess the evolution of the stiffness of the elastic and collagen fiber networks respectively. We then calculated the hysteresis area of cycles 1 and 3, to estimate the dissipated energy through irreversible damage and viscous phenomena. Hysteresis area is calculated as the difference between the area under the load curve (stored energy) and the area under the unload curve (restored energy) of the stress-stretch curve. Finally, we also assessed rupture properties by measuring the rupture stretch and stress for the last image taken before the sample broke.

All mechanical test raw data are archived at the Columbia University Librarys digital repository Academic Commons (doi: http://GET A DOI).

### 2.5. Statistical analysis

One-way ANOVA tests were used to establish statistical significance between groups for the different mechanical parameters assessed. Groups showing a p-value less than 0.05 were considered statistically significant.

## 3. Results

### 3.1. Geometry

From early pregnancy (gestation day 6) to one day before birth (gestation day 18) the cervix nearly doubles in size (Table 1). Interestingly, we observe a small contraction of the cervix size in the earliest stage of pregnancy, as d6 samples are noticeably smaller than NP samples. An overview of the initial measured dimensions all cervix types, measured after swelling and averaged over the 5 samples for each group (± standard deviation) is given in Table 1. There is no important geometrical variation between samples within the late pregnancy groups (d15, d18, d15-LPS sham, d15-LPS and d15-RU486).

### 3.2. Tangent moduli at low and high stretch

Considering the cervix has a strong non-linear hyperviscoelastic material behavior and the measured mechanical characteristics will depend on loading history, the comparison of mechanical properties between loading groups (i.e. NP/early pregnancy, mid-pregnancy, and late pregnancy) must be carried out with caution. Comparisons within the same loading group can be made and additionally, since the first series of cycles is common between all loading groups, the parameters of this series can be directly compared.

The mechanical response of all mouse cervical samples tested had the expected non-linear behavior with loading. A representative cyclic mechanical response for a d15-LPS treated sample is illustrated in Fig. 4, while the remaining representative sample curves are provided as supplementary data. This non-linear loading behavior resembles a J-shaped curve, with an initial linear toe-region followed by an upturn in mechanical response to a stiffer linear region. During unloading, the mechanical response followed the same J-shaped curve, but with a smaller magnitude of load compared to loading at the same stretch level. Hence, hysteresis is present in the mechanical response to load and unload. The mechanical response is also consistently shifted to the right on the stress-stretch curve between two successive cycles, indicating a combination of damage mechanisms of the sample, that we quantify with the stretch shift parameter $\Delta\lambda$. As mentioned, the stretch shift measurement, besides being an indication of damage, could include some preconditioning effects and the Mullins effect observed on soft tissues, especially for the first series of loading. However, those effects are believed to be minimal since we see a very limited hysteresis attenuation between cycle 1 and 3 (Fig. 4), indicating that the main phenomenon contributing to the stretch shift comes from true damage to the structure. Additionally, since we do not cut open our cylindrical samples which are still intact at the moment of testing, we expect the traditional preconditioning effects coming from a particular sample explantation/preparation to be minimal.

A measure of stiffness that is directly comparable between the specimen groups is the $E_{max}$ at the first loading level of 0.05N, reported in Fig. 5, because all samples see the same loading history. We observe a statistically significant stiffening of the cervical tissue between NP and d6 samples. This initial stiffening is followed by a significant softening up to d12, which continues up to d18. A difference in the degree of softening between d12 and d15 samples is not significant, though the extent of softening between d12 and d18 is statistically significant. When comparing samples in the late pregnancy and PTB groups, there is significant difference in $E_{max}$ measured at 0.05N between the d12 samples and d15-RU486 but not d15-LPS samples. The d15-LPS sham group trended towards a slightly higher $E_{max}$ than the other groups with a greater variability among samples. It is interesting to note, because NP and d6 samples are much stiffer than the rest of the pregnant samples, the tangent moduli $E_{max}$ at 0.05N for these samples are measured in the toe region of the mechanical response. Whereas this tangent modulus for the other pregnant samples is measured in the stiff region past the toe of the J-shaped mechanical response. The small deformation region is typically associated with the elastic fiber contribution, whereas the stiff region is typically associated with the contribution of collagen fibers.

When comparing $E_{max}$ tangent moduli between cycles at different loading levels within each specimen group, stiffness increases with increased load levels as expected for a non-linear material (Fig. 6a, $E_{max}$ calculated on cycle 1 for all load series). The evolution of $E_{max}$ calculated on cycle 1 for all load series (Fig. 6a) confirms the early stiffening identified between NP and d6, even at high loading level when the samples are loaded outside of the toe-region. When focusing on the late pregnancy group (Fig. 6b), there was no statistically significant differences between the d15 and d18 tissue, nor the untreated d15 and the d15-LPS and d15-RU486 treated samples. It is noted here that the tangent moduli evolution with increasing load levels is not much different between specimens in the late pregnancy group. Along with reporting $E_{max}$, Fig. 6 also reports the number of specimens (out of n=5 for each) that completed each load cycle without breaking. A further explanation of these rupture results is in Section 3.4.

On average, the low stretch modulus $E_0$ presents a similar trend to the $E_{max}$, with the identification of stiffening in the early pregnancy stage between NP and d6 and decline in mid-pregnancy through to late pregnancy (Fig. 7a). The NP and d6 samples have more variability in this parameter than the late pregnancy group and $E_0$ declines with higher loading levels starting at the 1N load cycles.

Focusing on the late pregnancy group, which all see the same lower magnitude loading history, the moduli at low stretch $E_0$ stays constant within each specimen group at the different loading levels (Fig. 7a). Since the low stretch modulus $E_0$ does not vary much with the loading level, it was averaged over all cycles of all series (Fig. 7b). Contrary to $E_{max}$, the averaged low stretch modulus $\overline{E_0}$ presents statistically significant differences between specimen within the late pregnancy group, and thus is the most distinct mechanical parameter between specimen groups. Indeed, d18 and d15-RU486 $\overline{E_0}$ are significantly different from d15 and d15-LPS sham (Fig. 7b), while d15-LPS $\overline{E_0}$ is in between. The average modulus $\overline{E_0}$ is 4.6e-4 ± 0.9e-4MPa and 5.5e-4 ± 1.2e-4MPa for d15 and d15-LPS sham and significantly drops to 2.6e-4 ± 0.5e-4MPa and 2.6e-4 ± 1.2e-4MPa for d18 and d15-RU486.

### 3.3. Damage parameters

Globally, all specimen groups showed an increased stretch shift Δλ with increasing loading level (Fig. 8). The exception of d6 and d15-LPS for the 5th series is likely due to the fact that all the samples did not reach the 5th series. While a direct comparison is prohibited between the absolute levels of early and late pregnancy groups, the lower levels on average of the NP and d6 groups compared to late pregnancy suggest there is an overall less permanent deformation for those samples, although they have been loaded to higher load levels. The comparison of the first series stretch shift highlights this point since almost no permanent deformation is observed for NP, d6 (and even d12 relatively), while the late pregnancy group already shows high stretch shifts (particularly d18, d15-LPS and d15-RU486).

Similar to the gestation day 18, the PTB models have a higher stretch shift on average for all series compared to d15 and d15-LPS sham. For instance, for the first series, the stretch shift increases significantly from 0.04 ± 0.02 for d15 and d15-LPS sham to 0.11 ± 0.03, 0.10 ± 0.03, 0.11 ± 0.06 for d18, d15-LPS and d15-RU486 respectively.

The hysteresis area, associated with the dissipated energy, increases with increasing load levels for all specimen groups (Fig. 9). The dissipated energy on cycle 3 consistently trends lower than the energy dissipated on cycle 1 within a same series, for all specimen groups, suggesting some irreversible reorganization of the cervical ECM after the first cycle of each series. There are no statistically significant differences in the hysteresis area between the samples of the late pregnancy group (Fig. 9). Indeed, the levels of dissipated energy are similar between the different specimen groups for all series.

### 3.4. Rupture parameters

Parameters that allow assessment of a tissues rupture properties include the stress at rupture, the stretch at rupture and the number of samples that complete the cyclic loading regime prior to tissue failure. A direct comparison of rupture properties between specimen groups cannot be made since each group experienced different loading levels. However, qualitatively, cervices from the NP and early pregnancy group appear to be much stronger than late pregnancy samples, demonstrated by the higher stress levels reached before rupture (Fig. 10a). Cervices from the late pregnancy group also show an increased extensibility as they break at higher stretch levels ($\lambda_{rupture}$ around 5 while it is only around 2.5 for NP and d6, Fig. 10b). While no significant difference in rupture stress or rupture stretch was identified in the late pregnancy group between the day 15, day 15-PTB (LPS or RU486), and term pregnant (d18), both PTB models had a reduced number of cervices that were able to complete the cyclic loading regime. From all the specimen groups, d15-LPS samples presents the lowest rupture stress (Fig. 10a). All five d18 samples made it through the entire cyclic testing regimen. However, not all of the d15-LPS and d15-RU486 treated samples completed the cyclic loading, with the d15-LPS samples performing the worst since only 3 out of 5 samples made it to the 0.3N loading level and only 1 sample made it to the 0.4N load level (Fig. 8).

## 4. Discussion

In this study, we report the evolution of cervical mechanical properties along normal and abnormal pregnancy. Through cyclic mechanical testing, we quantitatively show certain features of the mechanical behaviour of the pregnant mouse cervix are uniquely altered by infection (LPS-treatment). This mechanical testing evidence parallels previous studies [26, 27, 24, 25] showing infectionmediated tissue remodeling is regulated by a distinct pathway as compared to progesterone withdrawal mediated premature and term remodeling. The cyclic tensile test performed here enables assessment of the cervix s ability to accommodate loading and provides an estimate of the evolving damage mechanical state of the sample with increasing load level.

Previous studies have established the mechanical response of the pregnant mouse cervix to a classic load-to-break mechanical test [17, 12, 27, 15, 32] and have quantified the drastic

material remodeling that occurs during the course of a normal pregnancy. To establish a biomechanical signature that is able to distinguish the relative contribution of extracellular matrix (ECM) components involved with term and preterm remodeling, we extend previous mechanical characterization efforts and quantify the cyclic mechanical behavior of mouse cervical tissue samples. These tests provide insight as to how the microstructural modifications identified in biological studies impact the mechanical functionality of the tissue over the course of a normal pregnancy and in a premature birth (PTB). To this end, we developed a specific cyclic biomechanical test which allows delineation of mechanical properties associated with the state of the collagen fibers network as well as the elastic fibers network.

### 4.1. Loading in pregnancy

The in *vivo* physiological magnitude and pattern of stress and stretch of a cervix in the human and mouse are not entirely known. In the human, loading on the cervix arises from push of the fetal sac on the internal os (i.e. the top opening of the cervix into the uterine cavity), the pull of the stretched uterine wall, and pressure variations due to fluid and fetal movements [33, 34, 35]. As gestation progresses the magnitude of this load on the cervix grows. The mouse cervix most likely shares these common external loading features as in human pregnancy. However, mice are quadrupeds and they do not experience gravity in the same way humans do during pregnancy. The similarities and differences in the mechanical loading state between a mouse and human cervix remain to be determined. Nevertheless, studying the mechanical properties of the mouse cervix has merit because the state of cervical stress seen during extreme loading events are most likely conserved and as mentioned above in Section 1, tissue remodeling features of the collagen network in pregnancy are conserved between human and mice.

At the time of delivery, we hypothesize the mouse cervix experiences severe circumferential tensile stretches around the inner canal through the passing of the pups. Similar to human, the magnitude of loading depends greatly on the size and shape of the fetal sac, with the distinction that mice usually deliver between 6–10 pups. A cyclic tensile loading to extreme load levels seems therefore appropriate to model an actual delivery loading scenario. Considering the average circumferential size of a pup head at the time of delivery is around 25mm [36], we can estimate the stretch level induced by the passing of a pup into the cervical canal. The average cervical opening measurement of a d18 cervix in an undeformed state is 1.32 ± 0.09mm (Table 1), so a corresponding circumference of 4.1mm. A rough estimate of the corresponding stretch level associated with delivery is therefore around 6, which is slightly past the rupture stretch levels found in this study. It suggests at the time of delivery (early d19) the cervix is even more compliant than the d18 cervices we tested, and/or, since the pups are not completely rigid and might deform during delivery, the actual cervical stretch level at delivery might be lower than this estimate. Whatever the case, the stretch levels associated with delivery are extreme and should be put in relation to the highest stretch levels used here in the 4th and 5th series of loading.

### 4.2. Evolution of cervical mechanical properties during normal pregnancy

The dimensions of the cervix evolve considerably with advancing gestation, which emphasizes the importance of normalization of the mechanical measurements by geometry (Table 1). While the increase in cervix volume between early and late pregnancy is expected considering the function of the cervix at delivery, the initial small reduction in cervical dimensions between NP and d6 is associated with a different phenomenon than the overall softening process that begins shortly after day 6 and continues for the reminder of pregnancy. Previous load-to-break studies have not evaluated cervical mechanical properties at time points prior to gestation day 10 [12, 14, 32]. The increase in both $E_{max}$ (Fig. 6a) and $E_0$ (Fig. 7a) between NP and d6 indicates that before the softening phase in pregnancy, an initial stiffening phase of both the collagen and elastic fibers network occurs at this early stage of pregnancy. Harkness and Nightingale [37] previously reported a similar phenomenon in the rat cervix when they noticed a reduced extensibility of day 10 cervices (over a 21 day gestation) compared to NP, followed by the increasing extensibility associated to the softening stage. IFEA (Inverse Finite Element Analysis) conducted by Yoshida *et al.* [10] of load-hold mechanical tests also identified a stiffening of the ground substance associated to the elastic part of the material response between NP and d6 mice cervices.

The association of the low stretch modulus in uni-axial tensile experiments to the elastic fibers contribution is now well established in the literature since the early work on elastic arteries of Roach and Burton [38], and especially thanks to studies experimenting with elastase treatment showing the systematic association of a decrease in low stretch modulus with a degradation of elastin [39, 28]. The observed drop of $E_0$ with increasing load for NP, d6 and d12 suggests that the elastic part of the ECM is getting damaged with increasing load level. Secondly, the small initial stretch shift of 9e-3 ± 8e-3 and −7e-3 ± 8e-3 for NP and d6, respectively, in the first load series up to 0.05N (Fig. 8), is consistent with the relatively high $E_0$ of 1.7e-2 ± 1.5e-2MPa and 5.6e-2 ± 2.7MPa for these groups. These results indicate the elastic fiber network in both NP and early pregnancy is intact and can provide the tissue with great elasticity, taking it back to its original configuration after deformation at lower loads. Increased loading to the NP and d6 cervices caused an increase in the stretch shift thus providing further evidence that the elastic part of the ECM is damaged during the loading series causing permanent deformation to the tissue. Once again the stretch shift includes a combination of various deformation mechanisms, including collagen fibers uncrimping and slippage following elastin and crosslinks damage. Future studies will focus on differentiating the relative contribution of these different mechanisms.

Interestingly, for the late pregnancy group the observed trend for $E_0$, as seen for NP, d6 and d12 samples, is not present. Instead, we see a rather constant low value for $E_0$ suggesting that the elastic part of the tissue no longer contributes significantly to the mechanical response, and is not further damaged by the implemented loading scenario. This is enforced by the high stretch shift around 0.1 for the late pregnancy group at the beginning which indicates that the elastic fiber network does not have the ability to make the tissue recoil back to its original configuration after deformation. This concurs with reported microstructural observations showing that elastic fibers in mouse cervix appear intact up to

d12 (as seen on TEM images) and are remodeled to appear as condensed shorter fibers by d15 which is most pronounced by gestation d18 [15, 25].

The evolution of the $E_{max}$ tangent moduli across all groups clearly highlights the dramatic tissue softening up to d12, followed by a moderate softening up to d18 (Fig. 5). This finding is in agreement with the evolving cervical stiffness previously reported [15, 12, 17], which at the molecular level is achieved by the turnover of mature, crosslinked collagen with immature, poorly crosslinked collagen. The decline in collagen crosslinks corresponds directly to the decline in stiffness from gestation day 12 to day 15 and thereafter the moderate change in softening up to gestation d18 is not accompanied by a further reduction in collagen crosslink density [17, 9].

### 4.3. Mechanical signatures of infection- and hormone withdrawal-mediated premature tissue remodeling

The biochemical pathways by which premature cervical ripening is induced are different between the infection-mediated d15-LPS and the hormone withdrawalmediated d15-RU486 [26, 27, 25]. Collectively the biochemical studies also suggest that d15-RU486 preterm and d18 term are similar but not identical while premature cervical remodeling with d15-LPS is dissimilar from both term and the d15-RU486 PTB model. Recent transcriptomic studies further highlight the marked differences in the transcriptional pathways that direct term and LPS-mediated preterm cervical remodeling [24]. Of particular relevance is the noted increase in proteases that target collagen and elastic fibers in the d15-LPS group. The observed molecular distinctions between the two PTB models and term are reflected in microstructural reorganization of collagen and elastic fibers as observed by second harmonic generation imaging (SHG) and transmission electron microscopy (TEM) respectively. Compared to the NP cervix, collagen fibers and collagen fibrils undergo a progressive change in structure from early to late pregnancy. Collagen fibers and fibrils undergo a similar reorganization in the RU486-treated animals albeit the disorganization is more dramatic than the disorganization observed in gestation d18 term pregnant cervices (Fig. 11a). While collagen fibril organization appears unaltered in the cervix of d15-LPS group as observed in TEM images (Fig. 11a), collagen fiber structure undergoes region-specific alterations as identified by SHG [25].

In addition to changes in collagen architecture, there is also a distinct difference in elastic fibers ultrastructure between specimens of the late pregnancy group as seen on TEM images (Fig. 11b). Compared to the elastic fibers of d15 and d15-LPS sham, the d15-LPS tissue have disrupted elastic fibers with elastin not being properly integrated in the microfibrillar scaffold of the elastic fibers [24](Fig. 11b). On d18 of a term pregnancy, the elastic fibers are drastically remodeled compared to early/mid pregnancy with elastic fibers appearing shorter in a reorganized network but not disrupted [15]. Unpublished observations of d15-RU486 elastic fibers identify a range of different fiber “types”, with most of the fibers being similar to d15 and d18 groups, but some appearing disrupted as the ones in d15-LPS group. One aim of the present study is therefore to elucidate if these differences in microstructures result in distinct mechanical signatures for the d15-LPS and d15-RU486 models with specific mechanical properties in response to load-unload.

Of the mechanical parameters investigated in this study, $\overline{E_0}$ is the most distinctive parameter to differentiate specimens within the late pregnancy group (Fig. 7b). The significantly reduced $\overline{E_0}$ for d18 and d15-RU486 groups compared to d15 and d15-LPS sham suggests the elastic fiber network properties change significantly in late ripening, even more so than the collagen fibers, as the change of $E_{max}$ is more moderate for the late pregnancy group. Moreover, the reduced low-stretch modulus for the d18 and d15-RU486 tissue shows that it requires less force to stretch the tissue initially, suggesting less resistance from the elastic part of the tissue. Interestingly, $\overline{E_0}$ for d15-LPS is not significantly different from d15 and d15-LPS sham, in contrast to d18 and d15- RU486 (Fig. 7b). Integrating the microstructural observations with this distinct mechanical parameter, we suggest that the reorganized elastic fiber network of the term pregnant (d18) and the d15-RU486 preterm contributes to a decline in mechanical performance that is even greater than the decline in mechanical performance of the disrupted elastic fibers in the d15-LPS group. While not statistically significant the decline in $E_0$ and the low rupture stress (Fig. 10a) in the d15-LPS group along with the fact that only one specimen sustained the full loading regime (1 for d15-LPS, 3 for d15-RU486, 4 for d15 and d15-LPS sham and 5 for d18), suggest a contribution from the disrupted elastic fibers to the reduction in mechanical performance in this distinct model of PTB.

The observation that d15-LPS samples break easily concurs with recent transcriptome data which identified increased expression of proteases that target collagen and elastic fiber components (e.g. MMP13, MMP8) in the d15-LPS treated cervices but not in the term pregnant (d18). Also reported in this study is the observation of disrupted elastic fibers through TEM imaging [24]. Integrating these finding with the mechanical signature identified in the current study, the reduced mechanical strength is intuitively a logical result and provides functional evidence that the ECM is disrupted following LPS treatment and hence presents a weaker resistance to rupture. Interestingly, since the collagen fibers of d15-LPS undergo region-specific morphological changes that are modest compared to the d15-RU486 preterm and d18 term model, we suggest that not only collagen fibers but also elastic fibers have a significant contribution to the mechanical strength of the tissue. It is noteworthy that d15-RU486 and d18 have very similar mechanical properties ($E_{max}$, $E_0$, $\lambda_{rupture}$), enforcing the reported observations than d15-RU486 induces a cervical remodeling mimicking best what happens at term [26]. However, our results suggest that there are still slight differences in the mechanical behavior between d15-RU486 and d18 samples, as d15-RU486 samples appeared to be weaker than d18 since they broke earlier during loading.

Overall, d18, d15-RU486 and d15-LPS present mechanical properties similar to elastase treated samples, with namely, the important stretch shift and a very low $E_0$, once again suggesting that the elastic fiber network is the key difference between d15 and d15-LPS sham compared to d18 and the PTB models. Indeed, experiments conducted on aortas or ligaments subjected to an elastase treatment showed these tissues exhibit altered mechanical properties similar to our observations [39, 28, 40, 41]. Especially, Schriefl *et al.* [28] reports an increased remanent deformation and reduced initial stiffness for aortas treated with elastase subjected to cyclic uniaxial tests compared to control group. They attribute the remanent deformation to irreversible sliding of collagen fibers facilitated by the degradation of the elastic fibers. Indeed, despite the lack of elastin, the tissue still exhibits the non-linear

stiffening with increasing stretch associated to the gradual recruitment of collagen fibers, and possesses enough elasticity to retract after deformation but not completely causing permanent tissue elongation. It is likely we observe a similar phenomenon here, where the reorganized or disrupted elastic fibers in d18, d15-RU486 and d15-LPS do not contribute much to the mechanical response of the cervix, not preventing collagen fiber sliding and resulting in an increased stretch shift which increases with increasing load.

Experiments conducted on aortas of genetically altered mice lacking elastin (elastinKO) and/or key other proteins in elastic fibers assembly, showed the viscoelastic properties of elastinKO are also modified compared to control [30]. Indeed, besides the drop of low stretch modulus, the authors found that the energy dissipated during mechanical loading is increased in the elastinKO animals and so, not only elastin, but properly assembled elastic fibers are essential for a low energy dissipation. In our experiment, this difference in viscoelastic properties is not present within the late pregnancy group. Indeed, the d18, d15-RU486 and d15-LPS groups do not exhibit a significant difference in hysteresis area compared to the d15 and d15-LPS sham group (Fig. 9), suggesting that the difference in elastic fiber structure between those groups does not reflect on the viscoelastic properties of the tissues.

In the current study, we utilized a model of localized inflammation to the reproductive tract to mimic preterm birth resulting from an ascending infection. The corresponding control group was a sham surgery group (d15-LPS sham). While this control group does not have preterm birth, we consider this a model of sterile inflammation given the noted increase in proinflammatory cytokines and morphological changes in collagen fibers by SHG [24, 25]. Consistent with our previous observations that the d15-LPS sham is not identical to the d15 untreated group, the d15-LPS sham group presents a slightly increased stiffness compared to d15 that may be attributed to changes in collagen structure as the major increase is seen on $E_{max}$ (Fig. 6b). Thus the modest physiological changes that accompany sterile inflammation are reflected in the mechanical behavior.

The mechanical behavior identified in this study enforce the strong viscoelastic response of the cervix. These aspects must therefore be considered and included in constitutive models of the cervix to represent faithfully the actual behavior. The evolving mechanical state of the elastic fiber network is also another important feature of the cervix mechanical behavior with pregnancy. This feature of the behavior should be incorporated in constitutive modeling, for instance with the introduction of a damage function into the formulation of the strain energy, to account for mechanical as well as enzymatic degradation of the ECM [42].

### 4.4. Limitations

Given the challenging geometry of the mouse cervix and the difficulty in preparing defined and uniform mechanical testing specimens, this study presents limitations. First, there is a complex loading state applied to the entire cervix, which varies from a purely uni-axial tensile test. This limitation comes from the complex irregular geometry and small dimensions of the cervix throughout pregnancy that prevent running standard mechanical assays on well-defined sample geometry. The choice of doing a ring test was partly motivated to avoid cutting the sample open and potentially introducing damage during the

dissection process. Additionally, since all samples are subjected to the same preparation and loading type, comparisons can safely be made between the different specimen groups.

The assumption made on the cervix geometry which is idealized as a perfect cylinder to compute an averaged stress and stretch on the whole structure represents another limitation. Because performing a local, more accurate estimation of the stress-stretch state of the cervix during the test was too complex, we decided that the assessments made in this study were a good starting point to compare cervical mechanical properties between the different specimen types. During the test, the front and back inner surfaces of the sample remain mainly in contact, so that we do not see any transverse opening of the canal on the images of the side camera. Hence, the width measurement taken on those images correspond mostly to the additional thicknesses of the front and back wall, justifying our choice of cross section as Length*Width to calculate stress. Those combined limitations about the variation from a purely uniaxial tensile test and the idealized geometry imply that the tangent moduli identified in this study differ from usual standard material properties. However, the comparison of those mechanical parameters between our various specimen types, as well as their relation to microstructural events remain valid.

The definition of the reference configuration for the test represents a recurring problem when working on soft tissues characterization, as the *in vivo* state is very complex to characterize and replicate. Given that it might not be identical to the in vivo state, our reference configuration is taken after 3h of swelling in PBS and the application of a small pre-load for suture positioning, in order to have a consistent reference configuration between specimen groups. Waiting for a swelling equilibrium also ensures that the mechanical parameters assessed here are not influenced by a progressive water imbibing phase. Further studies are being conducted to investigate the influence of various solvents on the swelling mechanical response of the non-pregnant and gestation-timed pregnant cervical samples. Additionally, because the test is rather long (3h swelling + 5h for the loading scenario), we limited the data collection to 5 animals per specimen group. Additional tests should be conducted in order to increase the statistical power of the study presented here.

## 5. Conclusion

In this study, we characterize the mechanical response of the mouse cervix to a history of loading. The experimental work conducted expands our understanding of the evolution of cervical mechanical properties with advancing gestation. It also allows one to understand the changes in the late phase of cervical remodeling and identify distinctive alterations induced in hormone mediated and infection mediated PTB models. A cyclic test has been developed to tease out distinctive mechanical parameters of the cervix in normal and abnormal pregnancy at different gestation time points. Those parameters are then related to specific components of the ECM, namely the collagen and elastic fiber networks.

The main outcomes of this study are: i) in normal pregnancy, we identify an early stiffening phase between NP and d6, which precedes the softening phase identified at mid-pregnancy; ii) the main distinctive change in mechanical property between d15 and d18 cervices relates to the $E_0$ parameter, suggestive of the key importance of elastic fibers changes in late

pregnancy ripening; iii) PTB models and d18 tissues display reduced mechanical properties compared to d15 and d15-LPS sham; iv) premature cervical remodeling induced by RU486 on day 15 and term remodeling on d18 elicit very similar biomechanical signatures to cyclic loading, the only difference being that d15-RU486 are somewhat weaker; v) the d15-LPS appear weaker than d15-RU486 and d18, meaning they cannot withstand high levels of load-unload. Taken altogether, these findings provide a biomechanical assessment that uncovers phase specific contributions of the collagen and elastic fiber network to the progressive change in mechanical function of the cervix through normal pregnancy and provides functional insight into the distinct ECM perturbations that accompany two unique models of premature birth.

The identification of the cervix response to a load-unload type of loading is particularly relevant to human pregnancy. The ability of the cervix to recover from its loading history is critical for a successful term pregnancy, since we hypothesize that a patient with a cervix that is prone to permanent deformation and damage are at risk for cervical failure and PTB. The experiment conducted here suggests that a pathophysiological state caused by an infection (similar to the LPS model) leads to very poor mechanical performances with reduced recovery potential. Clinically, the premature loss of mechanical performance may translate into increased funneling or cervical shortening and subsequently preterm birth. Thus, improved understanding of changes to the cervical ECM microstructure and its impact on mechanical performance of the cervix will aid in the development of improved therapies for prevention of preterm birth.

## Supplementary Material

Refer to Web version on PubMed Central for supplementary material.

## 6. Acknowledgment

Research reported in this publication was supported by the National Science Foundation CAREER award (CMMI 1454412) to KM and the March of Dimes Prematurity Research Initiative (#21-FY14–131) and NIH R01 HD084695 to MM and NIH R01 HD088481 to KM and MM. The content is solely the responsibility of the authors and does not necessarily represent the official views of the National Science Foundation, the March of Dimes, nor the National Institutes of Health. Authors would like to thank Dr Joy Vink, Dr Helen Feltovich and Dr Ron Wapner for valuable discussions regarding the writing of this manuscript.

## References

[1]. Hamilton BE, Martin JA, Ventura SJ, Births: preliminary data for 2012., National vital statistics reports : from the Centers for Disease Control and Prevention, National Center for Health Statistics, National Vital Statistics System 62 (2013) 1–20.

[2]. Martin JA, Hamilton BE, Osterman MJK, Driscoll AK, Mathews TJ, Births: Final Data for 2015., National vital statistics reports : from the Centers for Disease Control and Prevention, National Center for Health Statistics, National Vital Statistics System 66 (2017) 1.

[3]. World health organization. preterm birth fact sheet [online] (mar. 2015)., 2015.

[4]. Cunningham FG, Leveno KJ, Bloom SL, Hauth JC, Rouse DJ, Spong CY, Williams Obstetrics 23rd Edition, 2010.

[5]. Vink J, Mourad M, The pathophysiology of human premature cervical remodeling resulting in spontaneous preterm birth: Where are we now?, Seminars in Perinatology (2017).

[6]. Myers KM, Feltovich H, Mazza E, Vink J, Bajka M, Wapner RJ, Hall TJ, House M, The mechanical role of the cervix in pregnancy., Journal of biomechanics 48 (2015) 1511–23. [PubMed: 25841293]

[7]. Timmons B, Akins M, Mahendroo M, Cervical remodeling during pregnancy and parturition, Trends in Endocrinology and Metabolism 21 (2010) 353–361. [PubMed: 20172738]

[8]. Mahendroo M, Cervical remodeling in term and preterm birth: Insights from an animal model, Reproduction 143 (2012) 429–438. [PubMed: 22344465]

[9]. Akins ML, Luby-Phelps K, Bank RA, Mahendroo M, Cervical Softening During Pregnancy: Regulated Changes in Collagen Cross-Linking and Composition of Matricellular Proteins in the Mouse, Biology of Reproduction 84 (2011) 1053–1062. [PubMed: 21248285]

[10]. Yoshida K, Mahendroo M, Vink J, Wapner R, Myers K, Material properties of mouse cervical tissue in normal gestation, Acta Biomaterialia 36 (2016) 195–209. [PubMed: 26961804]

[11]. Yoshida K, Reeves C, Vink J, Kitajewski J, Wapner R, Jiang H, Cremers S, Myers K, Cervical collagen network remodeling in normal pregnancy and disrupted parturition in Antxr2 deficient mice., Journal of biomechanical engineering 136 (2014) 021017. [PubMed: 24390076]

[12]. Barnum CE, Fey JL, Weiss SN, Barila G, Brown AG, Connizzo BK, Shetye SS, Elovitz MA, Soslowsky LJ, Tensile Mechanical Properties and Dynamic Collagen Fiber Re-Alignment of the Murine Cervix Are Dramatically Altered Throughout Pregnancy, Journal of Biomechanical Engineering 139 (2017) 061008.

[13]. Kokenyesi R, Armstrong LC, Agah A, Artal R, Bornstein P, Thrombospondin 2 Deficiency in Pregnant Mice Results in Premature Softening of the Uterine Cervix1, Biology of Reproduction 70 (2004) 385–390. [PubMed: 14561659]

[14]. Read CP, Word RA, Ruscheinsky MA, Timmons BC, Mahendroo MS, Cervical remodeling during pregnancy and parturition: molecular characterization of the softening phase in mice, Reproduction 134 (2007) 327–340. [PubMed: 17660242]

[15]. Nallasamy S, Yoshida K, Akins M, Myers K, Iozzo R, Mahendroo M, Steroid hormones are key modulators of tissue mechanical function via regulation of collagen and elastic fibers., Endocrinology (2017).

[16]. Word RA, Landrum CP, Timmons BC, Young SG, Mahendroo MS, Transgene Insertion on Mouse Chromosome 6 Impairs Function of the Uterine Cervix and Causes Failure of Parturition1, Biology of Reproduction 73 (2005) 1046–1056. [PubMed: 16034000]

[17]. Yoshida K, Jiang H, Kim MJ, Vink J, Cremers S, Paik D, Wapner R, Mahendroo M, Myers K, Quantitative evaluation of collagen crosslinks and corresponding tensile mechanical properties in mouse cervical tissue during normal pregnancy, PLoS ONE 9 (2014).

[18]. Akgul Y, Holt R, Mummert M, Word A, Mahendroo M, Dynamic changes in cervical glycosaminoglycan composition during normal pregnancy and preterm birth, Endocrinology 153 (2012) 3493–3503. [PubMed: 22529214]

[19]. Fung Y-C, Biomechanics, volume 12, Springer New York, New York, NY, 1993 URL: http://www.amazon.com/Biomechanics-Mechanical-Properties-Living-Tissues/dp/0387979476{%}5Cnhttp://link.springer.com/10.1007/978-1-4757-2257-4http://link.springer.com/10.1007/978-1-4757-2257-4. doi:10.1007/978-1-4757-2257-4.

[20]. Leppert PC, Anatomy and physiology of cervical ripening., Clinical obstetrics and gynecology 38 (1995) 267–79. [PubMed: 7554594]

[21]. Zhang Y, Akins ML, Murari K, Xi J, Li M-J, Luby-Phelps K, Mahendroo M, Li X, A compact fiber-optic SHG scanning endomicroscope and its application to visualize cervical remodeling during pregnancy, Proceedings of the National Academy of Sciences 109 (2012) 12878–12883.

[22]. Myers K, Socrate S, Tzeranis D, House M, Changes in the biochemical constituents and morphologic appearance of the human cervical stroma during pregnancy, European Journal of Obstetrics Gynecology and Reproductive Biology 144 (2009) 82–89.

[23]. Barone WR, Feola AJ, Moalli PA, Abramowitch SD, The effect of pregnancy and postpartum recovery on the viscoelastic behavior of the rat cervix, Journal of Mechanics in Medicine and Biology (2012).

[24]. Willcockson AR, Nandu T, Liu C-L, Nallasamy S, Kraus WL, Mahendroo M, Transcriptome signature identifies distinct cervical pathways induced in lipopolysaccharide-mediated preterm birth,, Biology of Reproduction 98 (2018) 408–421. [PubMed: 29281003]

[25]. Nallasamy S, Akins M, Tetreault B, Luby-Phelps K, Mahendroo M, Distinct reorganization of collagen architecture in lipopolysaccharide-mediated premature cervical remodeling, Biology of Reproduction 98 (2018) 63–74. [PubMed: 29161343]

[26]. Holt R, Timmons BC, Akgul Y, Akins ML, Mahendroo M, The molecular mechanisms of cervical ripening differ between term and preterm birth, Endocrinology 152 (2011) 1036–1046. [PubMed: 21209014]

[27]. Timmons BC, Reese J, Socrate S, Ehinger N, Paria BC, Milne GL, Akins ML, Auchus RJ, McIntire D, House M, Mahendroo M, Prostaglandins are essential for cervical ripening in LPS-Mediated preterm birth but not term or antiprogestin-driven preterm ripening, Endocrinology 155 (2014) 287–298. [PubMed: 24189143]

[28]. Schriefl AJ, Schmidt T, Balzani D, Sommer G, Holzapfel GA, Selective enzymatic removal of elastin and collagen from human abdominal aortas: Uniaxial mechanical response and constitutive modeling, Acta Biomaterialia 17 (2015) 125–136. [PubMed: 25623592]

[29]. Ferruzzi J, Bersi MR, Uman S, Yanagisawa H, Humphrey JD, Decreased Elastic Energy Storage, Not Increased Material Stiffness, Characterizes Central Artery Dysfunction in Fibulin-5 Deficiency Independent of Sex, Journal of Biomechanical Engineering 137 (2015) 31007.

[30]. Kim J, Staiculescu MC, Cocciolone AJ, Yanagisawa H, Mecham RP, Wagenseil JE, Crosslinked elastic fibers are necessary for low energy loss in the ascending aorta, 2017 URL: http://dx.doi.Org/10.1016/j.jbiomech.2017.07.011. doi:10.1016/j.jbiomech.2017.07.011.

[31]. Dudley DJ, Branch DW, Edwin SS, Mitchell MD, Induction of preterm birth in mice by RU486., Biology of reproduction 55 (1996) 992–5. [PubMed: 8902208]

[32]. Mahendroo MS, Porter A, Russell DW, Word RA, The Parturition Defect in Steroid $5\alpha$-Reductase Type 1 Knockout Mice Is Due to Impaired Cervical Ripening, Molecular Endocrinology 13 (1999) 981–992. [PubMed: 10379896]

[33]. Fernandez M, House M, Jambawalikar S, Zork N, Vink J, Wapner R, Myers K, Investigating the mechanical function of the cervix during pregnancy using finite element models derived from high-resolution 3D MRI, Computer Methods in Biomechanics and Biomedical Engineering 19 (2016) 404–417. [PubMed: 25970655]

[34]. Westervelt AR, Fernandez M, House M, Vink J, Nhan-Chang C-L, Wapner R, Myers KM, A Parameterized Ultrasound-Based Finite Element Analysis of the Mechanical Environment of Pregnancy, Journal of Biomechanical Engineering 139 (2017) 051004.

[35]. Verbruggen SW, Kainz B, Shelmerdine SC, Hajnal JV, Rutherford MA, Arthurs OJ, Phillips ATM, Nowlan NC, Stresses and strains on the human fetal skeleton during development., Journal of the Royal Society, Interface 15 (2018) 20170593.

[36]. Dilworth MR, Andersson I, Renshall LJ, Cowley E, Baker P, Greenwood S, Sibley CP, Wareing M, Sildenafil Citrate Increases Fetal Weight in a Mouse Model of Fetal Growth Restriction with a Normal Vascular Phenotype, PLoS ONE 8 (2013) e77748. [PubMed: 24204949]

[37]. Harkness RD, Nightingale MA, The extensibility of the cervix uteri of the rat at different times of pregnancy, The Journal of Physiology 160 (1962) 214–220. [PubMed: 13904720]

[38]. Roach MR, Burton AC, The reason for the shape of the distensibility curves of arteries., Canadian journal of biochemistry and physiology 35 (1957) 681–90. [PubMed: 13460788]

[39]. Weisbecker H, Viertler C, Pierce DM, Holzapfel G. a., The role of elastin and collagen in the softening behavior of the human thoracic aortic media., Journal of biomechanics 46 (2013) 1859–65. [PubMed: 23735660]

[40]. Henninger HB, Underwood CJ, Romney SJ, Davis GL, Weiss JA, Effect of elastin digestion on the quasi-static tensile response of medial collateral ligament, Journal of Orthopaedic Research 31 (2013) 1226–1233. [PubMed: 23553827]

[41]. Henninger HB, Valdez WR, Scott S. a., Weiss J. a., Elastin Governs the Mechanical Response of Medial Collateral Ligament Under Shear and Transverse Tensile Loading, Acta Biomaterialia (2015).

[42]. Robertson A, Hill M, Li D, Structurally motivated damage models for arterial walls. Theory and application, in: Ambrosi D, Quarteroni A, Rozza G (Eds.), Modeling of Physiological Flows SE - 6, volume 5 of *MS&A Modeling, Simulation and Applications*, Springer Milan, 2012, pp. 143–185. URL: 10.1007/978-88-470-1935-5{_}6. doi:10.1007/978-88-470-1935-5_6.

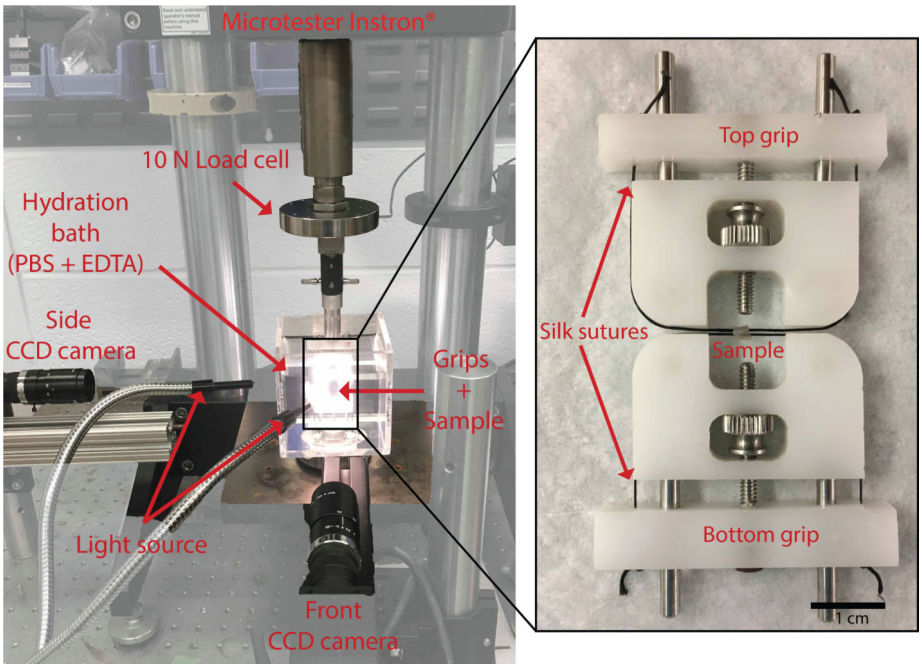


**Figure 1: Experimental set up.**

Mechanical testing set up (left panel) with a magnified view of the cylindrical sample mounted on the grips with silk sutures passed through the cervical canal. CCD camera views are in Figure3.

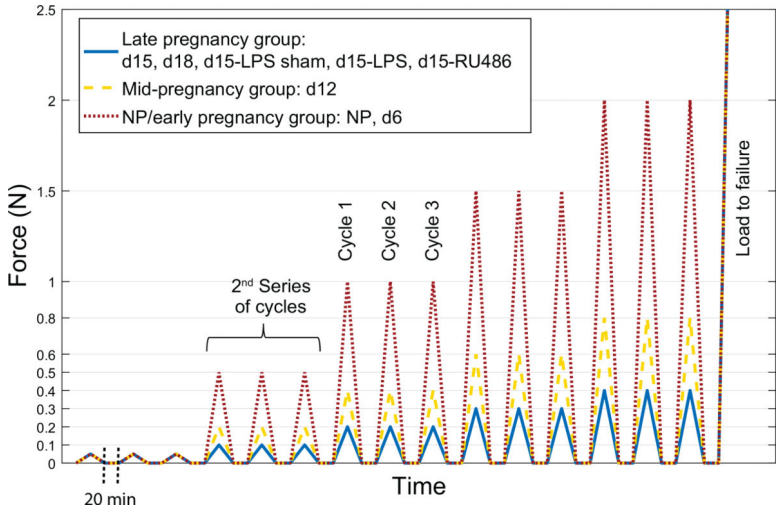


**Figure 2: Loading regimen of the displacement controlled load-unload test, for the 3 loading groups.**

NP/early pregnancy in dot/red (NP and d6), mid-pregnancy in dash/yellow (d12) and late pregnancy in line/blue (d15, d18, d15-LPS sham, d15-LPS and d15-RU486). Loading consists of 5 series with 3 cycles at different load levels, followed by load to failure. Loading is conducted at 0.1mm/s with 20min recovery between cycles (note: time is not to scale on graph).

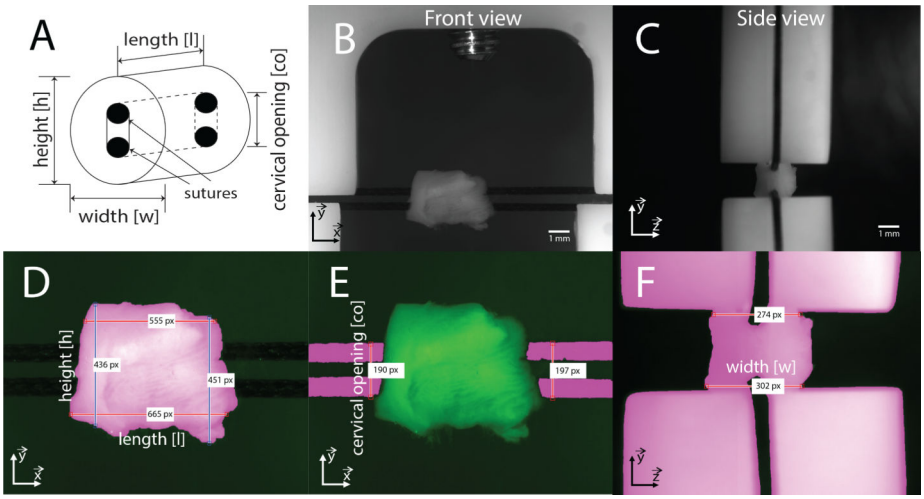


**Figure 3: CCD camera view and segmentation routine**

a) Definition of the geometry measurements. b-c) Example of the front and side view of the cameras. The traction direction $\vec{y}$ correspond to the vertical direction. d-e-f) Segmented images with indicated measurements. Pink area corresponds to the segmented part of the images while dark green is background. For length [*l*], height [*h*] and width [*w*], measurements were taken by counting the number of pixels at each horizontal pixel line of the image (or vertical line for height) in the segmented area between the two indicated boundaries (≈300–500 measurements), and averaged. Cervical opening [*co*] was defined as the average between right and left measurements.

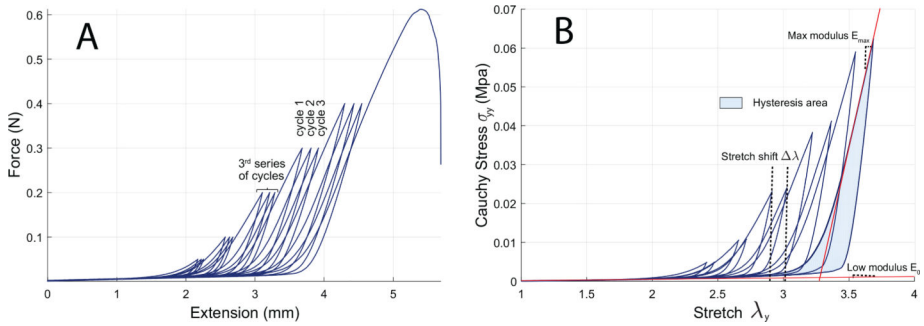


**Figure 4: Representative data from a d15-LPS sample.**

a) Example of force-extension raw data. b) Corresponding stress-stretch curve including the 1st and 3rd cycle of each loading series. Stretch shift Δλ is defined as the difference between peak stretches between cycles 1 and 3 of a same series. Hysteresis area is calculated as the difference between area beneath the loading curve and area beneath the unloading curve. Modulus at low and high stretch ($E_0$ and $E_{max}$) are computed on the loading curve. Representative raw data curves for the other specimen groups are included in supplementary figures.

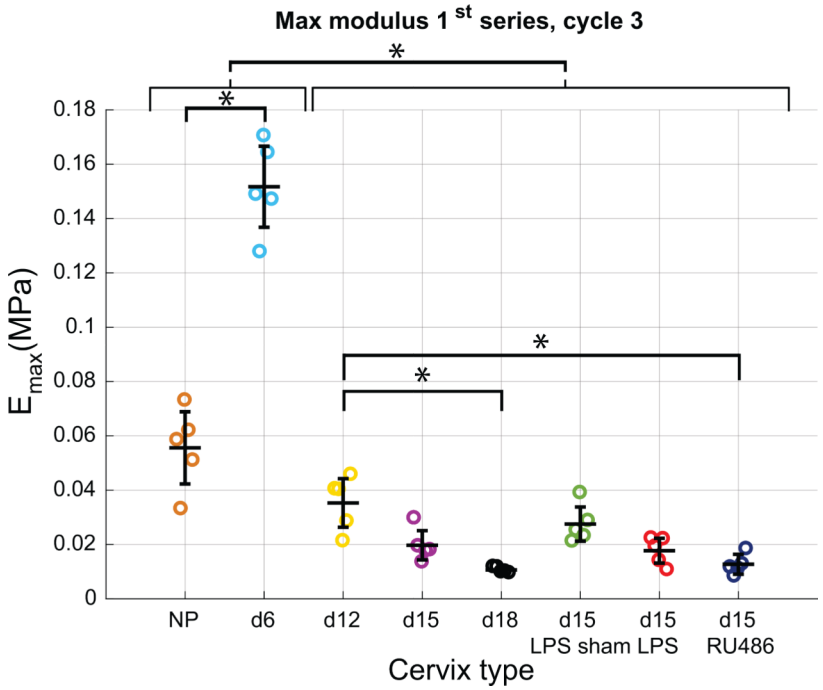


**Figure 5: $E_{max}$ with advancing gestation.**

Max modulus calculated on the loading curve of cycle 3 of the 1st series (common loading up to 0.05N for all specimen groups). Note that because of their greater stiffness, this modulus is calculated in the toe-region of the classical J-shaped curve for NP and day 6, since loading up to 0.05N is not enough to get out of this initial linear region for those groups. For the mid-pregnancy and late pregnancy groups, this modulus is calculated on the stiff part of the curve, past the toe-region. * indicates statistical significance between specimen groups (n=5, $p<0.05$).

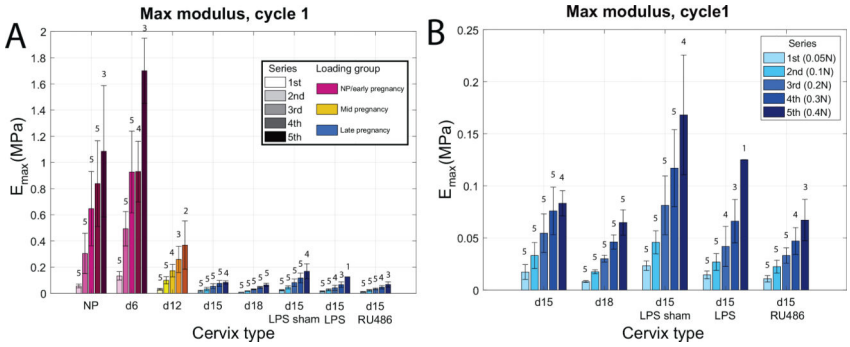


**Figure 6: Stiffening behavior with increasing load levels for each specimen group.**

a) Max modulus $E_{max}$ calculated on the loading curve of cycle 1 for all series. Note that all specimen groups are not subjected to the same loading (different colors). Numbers above bars indicate how many samples made it to the associated series of loading (out of n=5). b) Subset of panel A to focus on the late pregnancy group which were all subjected to the same loading regimen.

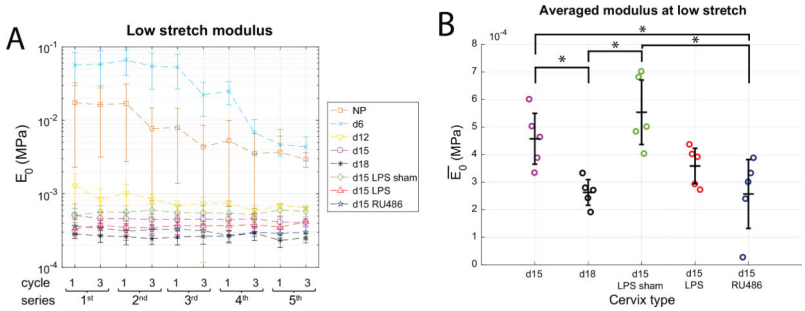


**Figure 7: Modulus measured at low stretch.**

a) Evolution of low stretch modulus $E_0$ between cycles and between load-level series (n=5). b) Modulus at low stretch averaged over all series $E_0$ and all samples within a group. Error bar is standard deviation relative to inter-sample variability. * shows statistical significance between groups (n=5, $p<0.05$). The modulus measured at low stretch gives an assessment of elastic fiber network in term and preterm pregnant cervical samples.

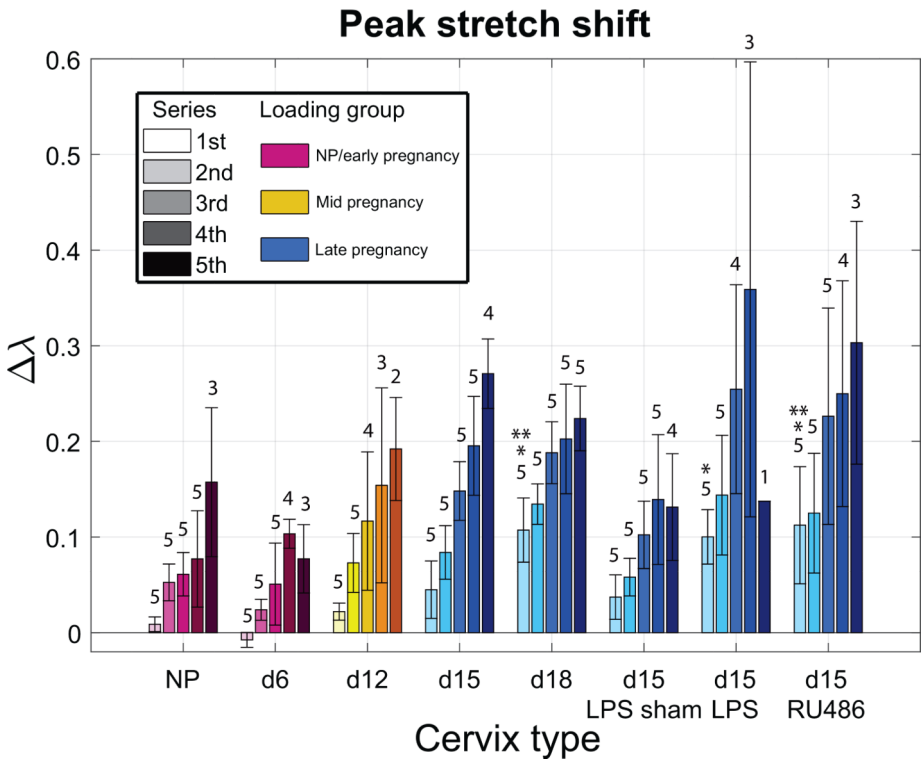


**Figure 8: Evolution of stretch shift parameter with loading for all specimen groups.**

Stretch shift Δλ for the different specimen groups calculated as the difference between peak stretch of cycle 1 and 3 for each series. Overall, there is an increase in permanent deformation for the d15 and d18 groups compared to NP, d6 and d12 indicated by the increase in stretch shift Δλ. Additionally, the PTB models and d18 have an increase in stretch shift compared to d15 and d15-LPS sham. Numbers indicate how many samples made it to the associated series (out of n=5). * indicates statistical significance compared to NP, d6 and d12 for the first load series ($p<0.05$). ** indicates statistical significance compared to d15 and d15-LPS sham for the first load series ($p<0.05$).

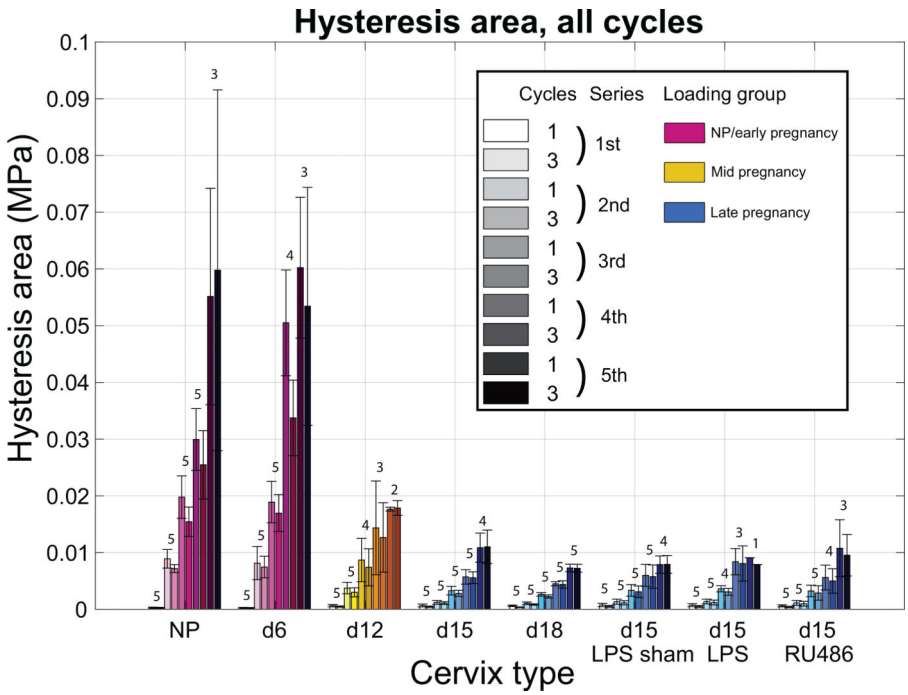


**Figure 9: Hysteresis area with increasing loading level.**

Hysteresis area calculated on the stress-stretch curve, for all cycles of loading and all the different specimen groups. Note that all specimen groups are not subjected to the same loading (different colors). Hysteresis area is associated with the energy dissipated during cyclic loading. Numbers above bars indicate how many samples made it to the associated series of loading (out of n=5).

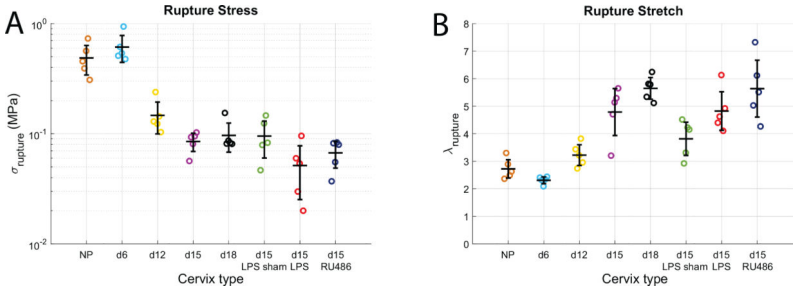


**Figure 10: Cervical rupture properties for term and preterm samples.**

Rupture stress (a) and stretch (b) for all specimen groups measured from the last image taken before the sample broke (n=5).

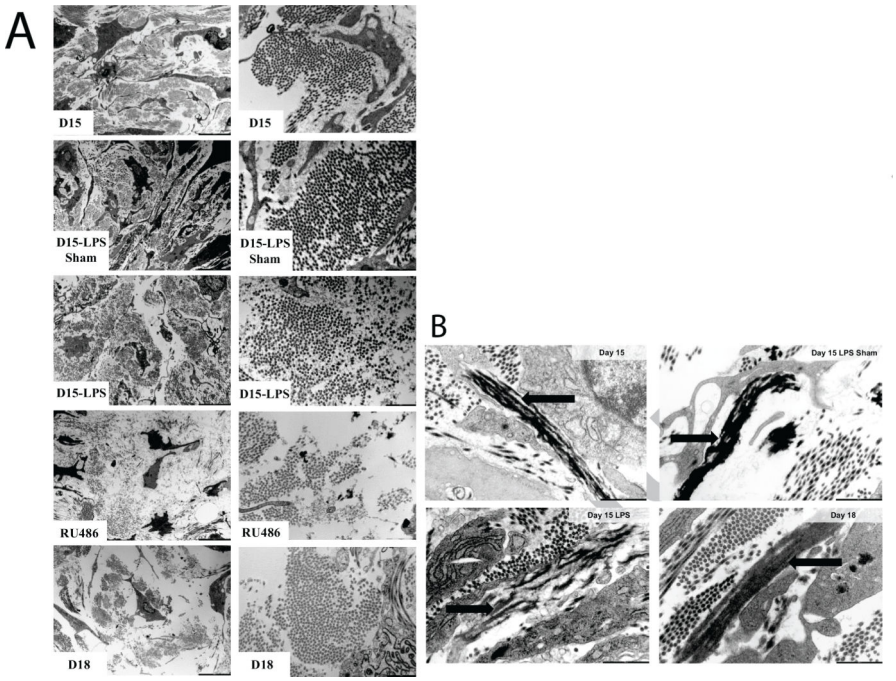


**Figure 11: Ultrastructural assessment of cervical collagen and elastic fibers organization through transmission electron microscopy imaging.**

a) Collagen fibers as seen on TEM images of cervical ECM taken on gestation d15, d15-LPS sham, d15-LPS, d15-RU486 (MFP) and d18. Left panel: 4200×; Right panel: 20500× magnification. Images reproduced from [15] with permission. b) Elastic fibers of cervical ECM observed through TEM for d15, d15-LPS sham, d15-LPS and d18 cervices. Black arrows indicate the elastic fibers ultrastructure which appears disrupted in d15-LPS, with elastin not being properly integrated in the microfibrillar scaffold of the elastic fibers compared to control. Scale bars are 1m. Images reproduced from [24] with permission.

**Table 1:**

**Initial cervical geometry measurements.**

Values are mean measurements over the different samples (n=5) ± SD. The initial geometry for each sample corresponds to the geometry of our reference configuration for the test and is measured on the first image taken after the 3h of swelling and the application of a small pre-load of 0.001N.

| Type | Initial measurement (mm) | | | |
|---|---|---|---|---|
| | Length | Height | Width | Cervical opening |
| NP | 3.43 ± 0.32 | 2.70 ± 0.20 | 2.60 ± 0.28 | 1.25 ± 0.11 |
| d6 | 2.65 ± 0.19 | 2.17 ± 0.15 | 2.12 ± 0.19 | 1.06 ± 0.07 |
| d12 | 3.59 ± 0.50 | 2.96 ± 0.47 | 2.86 ± 0.36 | 1.25 ± 0.14 |
| d15 | 4.19 ± 0.71 | 3.54 ± 0.34 | 3.78 ± 0.31 | 1.29 ± 0.07 |
| d18 | 5.15 ± 0.46 | 4.20 ± 0.58 | 4.59 ± 0.54 | 1.32 ± 0.09 |
| d15-LPS sham | 4.20 ± 0.23 | 3.41 ± 0.39 | 3.16 ± 0.35 | 1.38 ± 0.15 |
| d15-LPS | 4.49 ± 0.36 | 3.75 ± 0.13 | 4.36 ± 0.54 | 1.41 ± 0.08 |
| d15-FIU486 | 4.92 ± 0.21 | 4.12 ± 0.09 | 4.41 ± 0.37 | 1.53 ± 0.16 |